On the Applicability of Topological Methods for Complex Flow Data

Holger Theisel[1], Tino Weinkauf[2], Hans-Christian Hege[3], Hans-Peter Seidel[4]

[1] Bielefeld University, Germany. `theisel@techfak.uni-bielefeld.de`
[2] Zuse Institute Berlin (ZIB), Germany. `weinkauf@zib.de`
[3] Zuse Institute Berlin (ZIB), Germany. `hege@zib.de`
[4] MPI Informatik Saarbrücken, Germany. `hpseidel@mpi-inf.mpg.de`

Summary: In this paper we study the applicability of topological methods for creating expressive, feature revealing visualizations of 3D vector fields. 3D vector fields can become very complex by having a high number of critical points and separatrices. Moreover, they may have a very sparse topology due to a small number of critical points or their total absence. We show that classical topological methods based on the extraction of separation surfaces are poorly suited for creating expressive visualizations of topologically complex fields. We show this fact by pointing out that the number of sectors of different flow behavior grows quadratically with the number of critical points – contrary to 2D vector fields. Although this limits the applicability of topological methods to a certain degree, we demonstrate the extensibility of this limit by using further simplifying methods like saddle connectors. For 3D vector fields with a very sparse topology, topological visualizations may fail to reveal the features inherent to the field. We show how to overcome this problem for a certain class of flow fields by removing the ambient part of the flow.

1 Introduction

Topological methods are standard tools to visualizing 2D vector fields. They gained a rather high popularity because they offer to express even a complex flow behavior by only a limited number of graphical primitives. The main idea behind them is to segment the vector field into areas of different flow behavior. To do so, so-called separatrices, mainly starting from critical points, are extracted and visualized.

Topological methods for 2D vector fields have been introduced to the visualization community in [11]. Later they were extended to higher order critical points [23], boundary switch points [6], and closed separatrices [34]. In addition, topological methods have been applied to simplify [6, 7, 28, 29], smooth

[33], compress [17, 25, 16] and construct [24, 32] vector fields as well as to compute distance functions of them [15, 2, 26].

For 3D vector fields, there is a remarkable gap between the need for simplified visual representations of vector fields, the knowledge of topological concepts, and their application as a visual analysis tool. The need for simplified visual representations of 3D vector fields is even higher than for 2D vector fields, since 3D vector fields tend to have a significantly higher amount of information to be visualized. Also, topological concepts for 3D vector fields are well-understood. Nevertheless, there are only a few applications of topological methods for 3D vector fields. Similar to 2D vector fields, [12] proposed methods for detecting and classifying first order critical points by an eigenvalue/eigenvector analysis of the Jacobian matrix. A system for visualizing the topological skeleton of 3D vector fields has been presented in [9]. Topological skeletons of particular analytic 3D vector fields are extracted in [18, 10]. Mahrous et. al [20, 19] obtain a topological segmentation of a vector field by densely sampling stream lines over the field and clustering areas where a similar inflow/outflow behavior of the stream lines is observed. [27] and [31] extract and visualize the intersection curves of the separation surfaces to obtain less cluttered and more expressive visualizations.

Like every visualization technique, topological methods do not give expressive visualizations for all kinds of 3D vector data. In fact, topological methods are limited to rather moderate topological complexity which becomes manifest in the number of present topological features: if only very few features are present (or no features at all), topological methods fail. On the other hand, if there are too many topological features, topological methods fail as well because they produce cluttered visualizations which are hard (or even impossible) to interpret.

It is the purpose of this paper to study where the limits for applying topological methods are, and to present solutions to extend these limits in both directions. For the upper limit (i.e. the fact that topological methods fail if the data is too complex), a number of technical and perceptional reasons are known. Here we show that there is an additional theoretical reason which strongly limits 3D topology to rather simple data sets. This reason lies in the fast growing number of sectors of different flow behavior. We show that – contrary to 2D vector fields – the number of sectors of different flow behavior grows in the worst case quadratically with the number of present topological features (i.e. critical points). As a consequence of this, classical topological methods (focusing on extracting critical points and separation surfaces) are not relevant for topologically complex vector fields. Nevertheless, we show that for simplifying methods like saddle connectors [27], the upper limit is above the currently considered topological complexity. In fact, we apply topological methods to topologically far more complex vector fields than previously considered in the visualization community.

For the lower limit of topological methods (i.e. the fact that topological methods fail for a very poor topology), a simple and well-known solution to

move the topological complexity up to a range where expressive visualizations are possible is to remove the ambient part of the flow. We show that this approach can reveal important structures of certain types of flow.

The rest of the paper is organized as follows: section 2 recollects topological concepts for 3D vector fields and their visualization. Section 3 studies the upper limit of topological methods by counting the number of sectors of different flow behavior. Section 4 demonstrates at an example how topological methods can be applied to topologically more complex data sets. Section 5 presents and discusses a solution for dealing with data sets of a very low topological complexity. Section 6 draws conclusions.

2 3D Vector Field Topology and its Visualization

Topological structures of 3D vector fields are well-understood in the visualization community for many years [12, 1, 3, 21]. In this section, we collect the most important concepts and properties, and we review approaches to visualizing them.

2.1 Critical Points

Consider a 3D vector field

$$\mathbf{v}(x,y,z) = \begin{pmatrix} u(x,y,z) \\ v(x,y,z) \\ w(x,y,z) \end{pmatrix}. \tag{1}$$

A first order critical point $\mathbf{x}_0$ (i.e., $\mathbf{v}(\mathbf{x}_0) = \mathbf{0}$) can be classified by an eigenvalue/eigenvector analysis of the Jacobian matrix $\mathbf{J_v}(\mathbf{x}) = \nabla \mathbf{v}(\mathbf{x})$, iff $\det(\mathbf{J_v}(\mathbf{x}_0)) \neq 0$. Let $\lambda_1, \lambda_2, \lambda_3$ be the eigenvalues of $\mathbf{J_v}(\mathbf{x}_0)$ ordered according to their real parts, i.e. $Re(\lambda_1) \leq Re(\lambda_2) \leq Re(\lambda_3)$. Furthermore, let $\mathbf{e}_1, \mathbf{e}_2, \mathbf{e}_3$ be the corresponding eigenvectors. The sign of the real part of an eigenvalue λ_i denotes – together with the corresponding eigenvector $\mathbf{e}_i$ – the flow direction: Positive values represent an *outflow* and negative values an *inflow* behavior. This leads to the following classification of first order critical points:

Sources:	0	$<Re(\lambda_1){\leq}Re(\lambda_2){\leq}Re(\lambda_3)$	
Repelling saddles:	$Re(\lambda_1){<}$	0	$<Re(\lambda_2){\leq}Re(\lambda_3)$
Attracting saddles:	$Re(\lambda_1){\leq}Re(\lambda_2){<}$	0	$<Re(\lambda_3)$
Sinks:	$Re(\lambda_1){\leq}Re(\lambda_2){\leq}Re(\lambda_3){<}$	0	

Thus, sources and sinks consist of a complete outflow/inflow, while saddles have a mixture of both. A repelling saddle has one direction of inflow behavior (called *inflow direction*) and a plane in which a 2D outflow behavior occurs

(called *outflow plane*). Similar to this, an attracting saddle consists of an *outflow direction* and an *inflow plane*.

Each of the 4 classes above can be further divided into two stable subclasses by deciding whether or not imaginary parts in two of the eigenvalues are present ($\lambda_1, \lambda_2, \lambda_3$ are not ordered):

$$\text{Foci:} \qquad Im(\lambda_1) = 0 \quad \text{and} \quad Im(\lambda_2) = -Im(\lambda_3) \neq 0$$
$$\text{Nodes:} \qquad Im(\lambda_1) = Im(\lambda_2) = Im(\lambda_3) = 0$$

An iconic representation is an appropriate visualization for critical points, since vector fields usually contain a finite number of them. Several icons have been proposed in the literature, see [12, 9, 18, 10, 27]. Here we follow the approach of [31] and color the icons depending on the flow behavior: Attracting parts (inflow) are colored blue, while repelling parts (outflow) are colored red. Higher order critical points are not considered in this paper.

2.2 Separatrices

Separatrices are stream lines or stream surfaces which separate regions of different flow behavior. Different kinds of separatrices are possible: They can emanate from critical points or boundary switch curves, or they are closed separatrices without a specific emanating structure. However, in this paper we consider separatrices starting from critical points only.

Due to the homogeneous flow behavior around sources and sinks (either a complete outflow or inflow), they do not contribute to separatrices. Each saddle point creates two separatrices: Considering a repelling saddle $\mathbf{x}_R$, it creates one separation curve (which is a stream line starting in $\mathbf{x}_R$ in the inflow direction by backward integration) and a separation surface (which is a stream surface starting in the outflow plane by forward integration). A similar statement holds for attracting saddles. Since for the segmentation of a vector field into sectors of different flow behavior only the separation surfaces (and not the separation lines) contribute, we only consider separation surfaces in the following.

Contrary to the 2D case, separatrices of 3D vector fields can intersect in a number of stream lines called saddle connectors [27]. Saddle connectors start in the repelling plane of a repelling saddle and end in the attracting plane of an attracting saddle. [31] extends the concept of saddle connectors to boundary switch connectors which are the intersections of separatrices emanating from boundary switch curves.

3 Counting the Number of Sectors

We start with an analysis of existing 3D topological visualization approaches and consider the topological complexity of the treated data sets. Table 1

gives a collection of these techniques, including the topological complexity of the treated examples. We express this complexity by counting the number of critical points, boundary switch curves and separatrices which are present in the application. Table 1 does not intend to give an evaluation of the considered techniques because they focus on different data sets or incorporate other visualization techniques as well. However, table 1 reveals that most of the applications deal only with vector fields of a very low topological complexity. Only the recent papers [27] and [31] consider fairly complex data sets but conclude that classical topological methods are not appropriate there.

Table 1. 3D topological visualization approaches and their number of treated topological features; #cp: number of critical points; #scp: number of separatrices starting from critical points; #bsc: number of boundary switch curves; #sbsc: number of separatrices starting from boundary switch curves.

reference	#cp	#scp	#bsc	#sbsc
[12]	≈ 20	≈ 5	0	0
[9]	≈ 2	0	0	0
[18]	3	2	0	0
[20]	0	0	≈ 10	≈ 10
[19]	1	1	≈ 10	≈ 10
[27]	184	121	0	0
[31]	184	121	13	22
[this paper]	452	452	0	0

We search for reasons why up to now topological methods have been applied only to rather simple data sets. Two classes of reasons are already known [27]:

1. *Technical reason:* 3D topological methods involve the integration of stream surfaces which is computationally more involved, less stable, and less accurate than the integration of stream lines in 2D.
2. *Perceptional reason:* The sectors of different flow behavior may have a complicated shape and hide each other, making a visual analysis of them a cumbersome task. Figure 6 shows an example of a vector field consisting of 4 saddles which create 6 sectors of different flow behavior. Even for this rather low number of sectors we observe the hiding effect making it hard to distinguish the different sectors.

In recent years the first problem became more and more unimportant due to the dramatic increase of computing capacities and a number of new algorithmic solutions ([13], [8], [22], [30]). One solution for the second problem is the saddle connector approach [27] [31].

Now we show that there is a third reason that topological methods are limited to low-complexity vector fields. We show that – simply spoken – the number of sectors of different flow behavior grows fast when the topological complexity of the vector field increases. As a measure of topological complexity, we take the number of present saddle points. Since most considered data sets have a global index around zero, the number of saddles is approximately half the number of critical points. Then we get a

3. *Theoretical reason:* The number of sectors of different flow behavior grows in the worst case quadratically with the number of saddle points in a 3D vector field.

We show that this reason is a serious limitation of applying topological methods to 3D vector fields. To prove this reason, we present formulas to compute the number of sectors of different flow behavior. To see the differences, we do so both for 2D and 3D vector fields.

3.1 Sector counting for 2D vector fields

2D vector fields generally consist of sources, sinks and saddles where a saddle creates 4 separation curves [11]. We get

Property 1. Given a 2D vector field $\mathbf{v}_{n_S}$ consisting of n_S saddle points, the number $sec(\mathbf{v}_{n_S})$ of sectors of different flow behavior fulfills

$$sec(\mathbf{v}_{n_S}) \ \leq \ 3\,n_s + 1 \qquad (2)$$

where the equality in (2) can be reached.

Property 1 essentially says that the number of sectors grows linearly with the number of saddle points. To show it, we start with a vector field consisting of only one saddle, as shown in figure 1a. This saddle divides the domain into four sectors. Now we insert a new saddle as shown in figure 1b. Since the different sectors are separated by stream lines which must not intersect each other, a new saddle replaces one of the old sectors by 4 new sectors, thus increasing the total number of sectors by 3. This gives

$$sec(\mathbf{v}_{n_S+1}) \ \leq \ sec(\mathbf{v}_{n_S}) + 3, \qquad (3)$$

which is an inequality since separatrices may end in the same source/sink which reduces the number of sectors. Figure 1c illustrates this. (3) and $sec(\mathbf{v}_0) = 1$ gives (2). To complete the proof, we only have to show that the equality in (2) can be reached. To do so, we construct a vector field $\mathbf{v}_{n_S}$ with $sec(\mathbf{v}_{n_S}) = 3\,n_s + 1$. Figure 2 illustrates the construction of such a simple vector field.

Property 1 gives a reason why 2D topological methods are rather popular even for fairly complex vector fields: the number of sectors to be distinguished grows only slowly (in fact linearly) with the increasing of the topological complexity (i.e. the number of saddle points). As we will show now, this does not hold for 3D vector fields.

3.2 Sector counting for 3D vector fields

For 3D vector fields, the number of sectors of different flow behavior depends in the worst case quadratically on the number of saddle points. We formulate
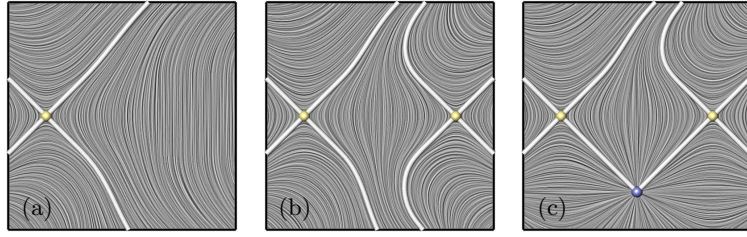
Fig. 1. (a) a single saddle point segments the domain into 4 sectors; (b) an additionally included saddle increases the total number of sectors by 3; (c) if separatrices end in the same source/sink, two sectors are merged.
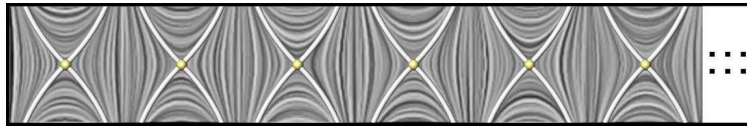
Fig. 2. Vector field $\mathbf{v}_{n_S}$ with $sec(\mathbf{v}_{n_S}) = 3\,n_s + 1$

Property 2. Given a 3D vector field $\mathbf{v}_{n_R,\,n_A}$ consisting of n_R repelling saddles and n_A attracting saddles, for the number $sec(\mathbf{v}_{n_R,\,n_A})$ of sectors of different flow behavior the inequality holds

$$sec(\mathbf{v}_{n_R,\,n_A}) \ \leq \ (n_R + 1)(n_A + 1) \tag{4}$$
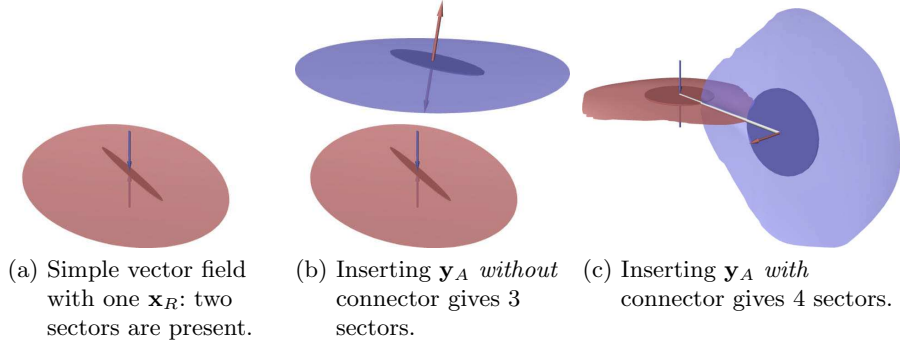
where the equality in (4) can be reached.

To show property 2, we start with a simple vector field $\mathbf{v}_{1,0}$ consisting only of one repelling saddle $\mathbf{x}_R$, as shown in figure 3a. The separation surface created by $\mathbf{x}_R$ divides $\mathbf{v}_{1,0}$ into two sectors. If we insert a new saddle, this can be either an attracting saddle $\mathbf{y}_A$ or a repelling saddle $\mathbf{y}_R$ as well. In the last case, the separation surfaces of $\mathbf{x}_R$ and $\mathbf{y}_R$ create three sectors of different flow behavior since they must not intersect. In case of a newly inserted attracting saddle $\mathbf{y}_A$, two cases are possible:

- The separation surface of $\mathbf{y}_A$ does not intersect the separation surface of $\mathbf{x}_R$. In this case, one of the old sectors is divided into two new sectors, and the total number of sectors is increased by 1. Figure 3b gives an illustration.
- The separation surface of $\mathbf{y}_A$ intersects the separation surface of $\mathbf{x}_R$. In this case, each of the two old sectors is divided into two new sectors. Thus, the total number of sectors is increased by 2. Figure 3c illustrates this.

As we can see from the simple example above, the total number of sectors does not only depend on the number of saddles but also on the number of saddle connectors.

For now we assume that every repelling saddle has a connector to every attracting saddle. Given a vector field $\mathbf{v}_{n_R,\,n_A}$, we consider the insertion of

(a) Simple vector field with one $\mathbf{x}_R$: two sectors are present.

(b) Inserting $\mathbf{y}_A$ *without* connector gives 3 sectors.

(c) Inserting $\mathbf{y}_A$ *with* connector gives 4 sectors.

Fig. 3. Correlation between number of sectors, saddles and connectors.

a new attracting saddle $\mathbf{x}_A$. Assuming that $\mathbf{x}_A$ has a connector to all n_R repelling saddles of $\mathbf{v}_{n_R,\,n_A}$, $\mathbf{x}_A$ divides $n_R + 1$ of the old sectors into two new sectors each. We get

$$sec(\mathbf{v}_{n_R,\,n_A+1}) \;\leq\; sec(\mathbf{v}_{n_R,\,n_A}) + n_R + 1 \tag{5}$$
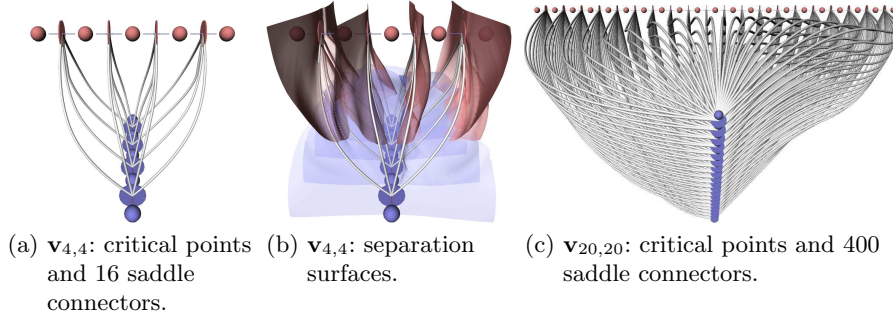
and in a similar way

$$sec(\mathbf{v}_{n_R+1,\,n_A}) \;\leq\; sec(\mathbf{v}_{n_R,\,n_A}) + n_A + 1. \tag{6}$$

(5), (6) and $sec(\mathbf{v}_{0,0}) = 1$ give (4).

To complete the proof of property 2, we construct an example vector field $\mathbf{v}_{n_R,\,n_A+1}$ with $sec(\mathbf{v}_{n_R,\,n_A}) = (n_R + 1)(n_A + 1)$. To do so, we use the topological vector field construction approach described in [32]. We place the n_R repelling saddles to the locations $(1, \frac{n_A}{2}, -d)$, $(2, \frac{n_A}{2}, -d)$, ..., $(n_R, \frac{n_A}{2}, -d)$ in such a way that the inflow plane of each saddle is parallel to the $y - z$ plane of the underlying Euclidian coordinate system. Furthermore, we place $n_R + 1$ sources at the locations $(0.5, \frac{n_A}{2}, -d)$, $(1.5, \frac{n_A}{2}, -d)$, ..., $(n_R+0.5, \frac{n_A}{2}, -d)$. To place the n_A attracting saddles, we choose the locations $(\frac{n_R}{2}, 1, d)$, $(\frac{n_R}{2}, 2, d)$, ..., $(\frac{n_R}{2}, n_A, d)$. In addition we place $n_A + 1$ sinks at the locations $(\frac{n_R}{2}, 0.5, d)$, $(\frac{n_R}{2}, 1.5, d)$, ..., $(\frac{n_R}{2}, n_A + 0.5, d)$. The positive number d describes the distance of the two rows of saddles. Figure 4a illustrates the location of the critical points for the example $\mathbf{v}_{4,4}$.

In the next step we have to construct a system of connectors such that each repelling saddle is connected to each attracting saddle. This is a set of $n_R \cdot n_A$ curves which must not intersect each other (except in the saddles themselves). Given the arrangement of critical points described above, this can easily be done as illustrated in figure 4a for $\mathbf{v}_{4,4}$. The complete constructed vector field ensures that for any source $\mathbf{x}_{So}$ and for any sink $\mathbf{x}_{Si}$ there are stream lines starting in $\mathbf{x}_{So}$ and ending in $\mathbf{x}_{Si}$. Figure 4b shows the complete topological skeleton of $\mathbf{v}_{4,4}$. Figure 4c shows an example of the constructed vector field $\mathbf{v}_{20,20}$ consisting of 441 sectors of different flow behavior.

(a) $\mathbf{v}_{4,4}$: critical points and 16 saddle connectors.

(b) $\mathbf{v}_{4,4}$: separation surfaces.

(c) $\mathbf{v}_{20,20}$: critical points and 400 saddle connectors.

Fig. 4. Constructed vector fields $\mathbf{v}_{4,4}$ and $\mathbf{v}_{20,20}$.

Property 2 can be concretized by incorporating not only the number of critical points but also the number of connectors:

Property 3. Given a 3D vector field $\mathbf{v}_{n_R, n_A, n_{Co}}$ consisting of n_R repelling saddles, n_A attracting saddles and n_{Co} saddle connectors, for the number $sec(\mathbf{v}_{n_R, n_A, n_{Co}})$ of sectors of different flow behavior the inequality holds

$$sec(\mathbf{v}_{n_R, n_A, n_{Co}}) \ \leq \ n_R + n_A + n_{Co} + 1. \tag{7}$$

To show property 3, we assume a vector field $\mathbf{v}_{n_R, n_A, n_{Co}}$ in which we insert a new attracting saddle $\mathbf{x}_A$. Further we assume that $\mathbf{x}_A$ creates m new saddle connectors, i.e. $\mathbf{x}_A$ is connected with m repelling saddles of $\mathbf{v}_{n_R, n_A, n_{Co}}$. In this case, $m+1$ sectors of the old vector field are divided into two new sectors each. We obtain

$$sec(\mathbf{v}_{n_R, n_A+1, n_{Co}+m}) \ \leq \ sec(\mathbf{v}_{n_R, n_A, n_{Co}}) + m + 1 \tag{8}$$

and in a similar way

$$sec(\mathbf{v}_{n_R+1, n_A, n_{Co}+m}) \ \leq \ sec(\mathbf{v}_{n_R, n_A, n_{Co}}) + m + 1. \tag{9}$$

This and $sec(\mathbf{v}_{0,0,0}) = 1$ gives (7).

Remarks:

1. The conditions in properties 2 and 3 are formulated as inequality because - similar to the 2D case - separatrices might end in the same critical points which leads to a reduction of the total number of sectors.
2. Properties 2 and 3 did not consider separatrices emanating from boundary switch curves. However, their quantitative behavior is similar to the separatrices from saddle connectors: the number of sectors grows in the worst case quadratically to the number of boundary switch curves.
3. Property 3 shows that in the best case the number of sectors grows linearly with the number of saddles. This happens if no saddle connectors exist at all. However, the example of the data sets in section 4 show that a higher number of saddle connectors usually exists.

4. Properties 2 and 3 considered at most one connector between a repelling saddle $\mathbf{x}_R$ and an attracting saddle $\mathbf{x}_A$. If multiple connectors are present, a sector (describing the flow from one particular source to one particular sink) may consist of different unconnected parts.
5. The sector counting presented here is a worst case estimation. Although an average case estimation would be useful, we are not aware of any approaches for this.

3.3 Interpretation of sector counting

From the sector counting approach in section 3 we draw the conclusion that classical 3D topological methods are limited to topologically rather simple vector fields. If the topological complexity (i.e. the number of saddles) grows, the number of sectors of different flow behavior very soon exceeds the limit of what can be distinguished in visualization. The only solution for this is to apply simplifying topological methods. The topological skeleton may be simplified by removing unimportant critical points or collapse clusters of critical points to a higher order one. While these methods are well-established for 2D vector fields ([6] [29]), we are not aware of any 3D extensions. The simplifying method we consider here are saddle connectors which we apply to more complex data sets in the next section.

4 Topologically Rich Vector Fields

From examples in [27] and [31] and from section 3 it is known that topological methods are hardly applicable for topologically complex vector fields. However, in this section we investigate topological methods for a 3D vector field of such a high topological complexity as it has – to the best of our knowledge – not been treated in the literature yet.

Figure 5 shows the transitional flow around a backward-facing step. The flow field is obtained from a numerical simulation of Kaltenbach and Janke at a Reynolds number of Re_H=3000 based on oncoming velocity and on step height. The corresponding boundary conditions are described in [14]. The data set contains 452 critical points which are visualized in figure 5a. Since the vector field is divergence-free, all of them are saddles.

A complete extraction and visualization of the separation surfaces was possible only at a very coarse resolution (figure 5b) since for higher resolutions the number of produced triangles very soon exceeded the limits of our available hardware. But even if we were able to process the complete skeleton at a high resolution, already figure 5a shows that an expressive topological visualization can not be achieved due to the sheer number of surfaces. Nevertheless, we were able to extract the intersection curves of these surfaces, namely the saddle connectors. As known from [27], this algorithm exhibits far less memory

consumption for both extraction and display than the treatment of separation surfaces themselves.

Figure 5d shows the visualization of the 1023 extracted saddle connectors. As we can see there, certain flow structures become visible: there are 3 rather independent clusters of turbulent flow behavior. However, it also shows that the segmentation property gets lost for vector fields of this complexity: no regions of different flow behavior can be distinguished any more from such a large number of saddle connectors. In fact, for complex data sets the approach of saddle connectors shifts from a topological segmentation techniques to a stream line selection technique.

Even if the complexity is too rich for a direct topological visualization, topological information can be used to parameterize other visualization techniques. We demonstrate this in figure 5e. Here, we made use of the extracted critical points and seeded stream lines close to them. This gives a far more expressive visualization than figure 5c, where stream lines have been seeded homogeneously over the whole domain. Both figures show the same number of stream lines.

Figure 5e illuminates the coherent structures of this type of flow: The flow separates at the corner of the step. The resulting shear layer rolls up in two Kelvin-Helmholtz vortices. In the downstream direction, the streamlines form bundles due to secondary streamwise vorticity. The fluid experiences a small backward flow in the upstream region below the shear layer.

5 Topologically Sparse Vector Fields

While dealing with a variety of data sets, we encountered vector fields where topological methods totally fail due to the absence of critical points and boundary switch curves. While it might not be possible to overcome this problem for all kinds of data, there is a solution for an important class of flow fields that exhibit a constant ambient flow part: all convections, i.e. coherent structures, move with nearly the same velocity and direction inside the flow. Their corresponding topological structures cannot be extracted since the ambient flow part cancels out the critical points. This clearly shows the Galilean-variance of topological examinations. By subtracting the ambient flow part, i.e. choosing a certain frame of reference, the coherent structures become visible using topological methods. To ensure meaningful results, this manipulation must be motivated by the physical interpretation of the data.

Consider the mixing layer visualized in figure 7a, where the flow moves downstream in both layers and the magnitude of the upper layer is three times larger than in the lower layer. The data set has been computed with a pseudo-spectral direct numerical simulation employing the computational domain and boundary conditions of Comte, Silvestrini & Bégou [4]. The Reynolds number is 100 based on the initial shear-layer thickness and convection velocity.

No critical points are present in this original frame of reference. In figure 7b we have chosen to subtract the constant vector field $(1, 0, 0)^T$. This yields the frame of reference where the flow in both layers has the same magnitude, but a different direction. The physical interpretation behind this manipulation is that we move as a observer with the same velocity and direction as the convections. The topology of this frame clearly shows formations of focus saddles indicating Kelvin-Helmholtz vortices, which alternate with formations of node saddles.

This example shows that topological methods yield expressive visualizations even for initially topologically sparse vector fields if a frame of reference can be chosen with regards to physical interpretation. Nevertheless, Galilean-invariant methods, like e.g. visualization of vortex regions, overcome the problem of finding the "right" frame of reference.

6 Conclusions

In this paper we made the following contributions:

- We have shown that – contrary to the 2D case – for 3D vector fields the number of sectors of different flow behavior grows in the worst case quadratically to the number of saddle points.
- We applied topological methods to more complex 3D vector fields than previously done in the literature.
- We have discussed that for some flow data of poor topological complexity, a removal of the ambient flow makes topological methods applicable.

We conclude that classical topological methods for 3D vector fields including critical points and separation surfaces are only of rather low relevance for most practical data sets. In fact, without simplifying methods like critical point clustering, critical point removing or saddle connectors, 3D topological methods won't get such a popularity as for 2D vector fields.

For saddle connectors we have shown that they are applicable to rather complex data, but from a certain complexity on the segmentation property gets lost, and saddle connectors are mainly perceived as stream lines.

For the future we expect an ongoing research on topology simplifying techniques because they seem the only promising way to make topological methods applicable to very complex 3D data sets.
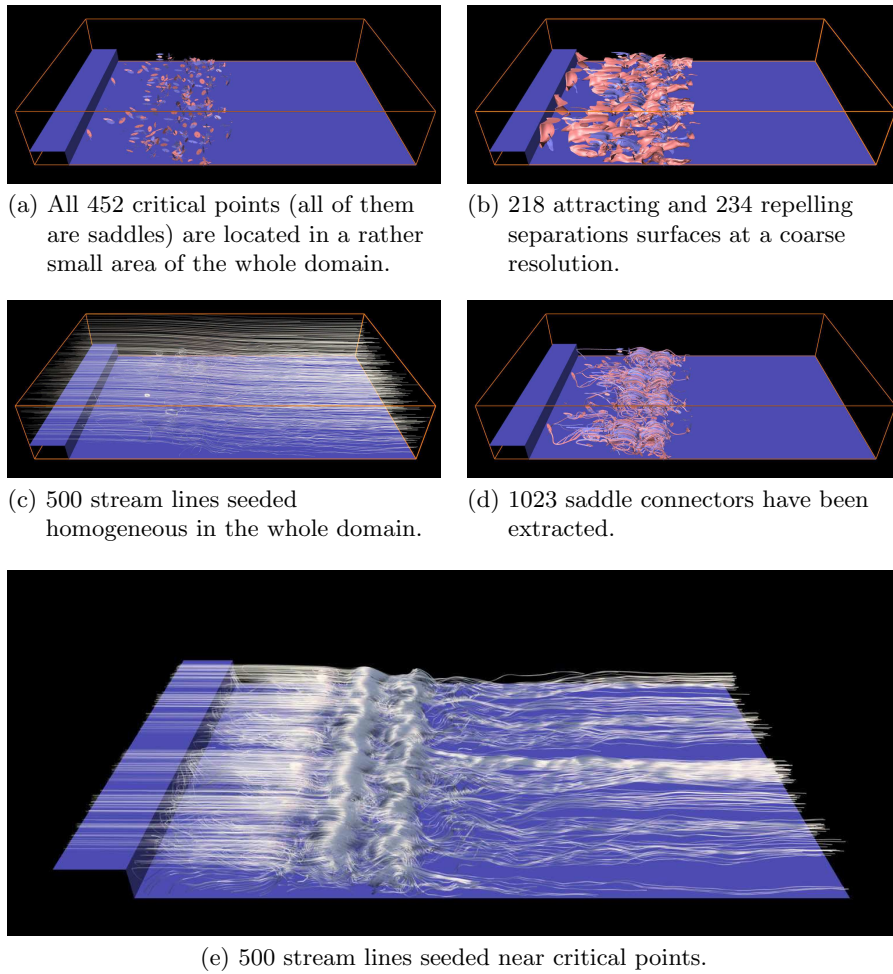
## Acknowledgements

References

1. D. Asimov. Notes on the topology of vector fields and flows. Technical report, NASA Ames Research Center, 1993. RNR-93-003.
2. R. Batra, K. Kling, and L. Hesselink. Topology based vector field comparison using graph methods. In *Proc. IEEE Visualization '99, Late Breaking Hot Topics*, pages 25–28, 1999.
3. M. S. Chong, A. E. Perry, and B. J. Cantwell. A general classification of three-dimensional flow fields. *Physics of Fluids A*, 2(5):765–777, 1990.
4. P. Comte, J.H. Silvestrini, and P. Bégou. Streamwise vortices in Large-Eddy Simulations of mixing layer. *Eur. J. Mech. B*, 17:615–637, 1998.
5. Stalling D, M. Westerhoff, and H.C. Hege. Amira: A highly interactive system for visual data analysis. *The Visualization Handbook*, pages 749–767, 2005.
6. W. de Leeuw and R. van Liere. Collapsing flow topology using area metrics. In *Proc. IEEE Visualization '99*, pages 149–354, 1999.
7. W. de Leeuw and R. van Liere. Visualization of global flow structures using multiple levels of topology. In *Data Visualization 1999. Proc. VisSym 99*, pages 45–52, 1999.
8. A. Van Gelder. Stream surface generation for fluid flow solutions on curvilinear grids. In *Data Visualization 2001. Proc. VisSym 01*, 2001.
9. A. Globus, C. Levit, and T. Lasinski. A tool for visualizing the topology of three-dimensional vector fields. In *Proc. IEEE Visualization '91*, pages 33–40, 1991.
10. H. Hauser and E. Gröller. Thorough insights by enhanced visualization of flow topology. In *9th international symposium on flow visualization*, 2000.
11. J. Helman and L. Hesselink. Representation and display of vector field topology in fluid flow data sets. *IEEE Computer*, 22(8):27–36, August 1989.
12. J. Helman and L. Hesselink. Visualizing vector field topology in fluid flows. *IEEE Computer Graphics and Applications*, 11:36–46, May 1991.
13. J. Hultquist. Constructing stream surfaces in steady 3D vector fields. In *Proc. IEEE Visualization '92*, pages 171–177, 1992.
14. H.-J. Kaltenbach and G. Janke. Direct numerical simulation of flow separation behind a swept, rearward-facing step at re_H=3000. *Physics of Fluids*, 12:2320–2337, 2000.
15. Y. Lavin, R.K. Batra, and L. Hesselink. Feature comparisons of vector fields using earth mover's distance. In *Proc. IEEE Visualization '98*, pages 103–109, 1998.
16. S. Lodha, N. Faaland, and J. Renteria. Topology preserving top-down compression of 2d vector fields using bintree and triangular quadtrees. *IEEE Transactions on Visualization and Computer Graphics*, 9(4):433–442, 2003.
17. S.K. Lodha, J.C. Renteria, and K.M. Roskin. Topology preserving compression of 2D vector fields. In *Proc. IEEE Visualization 2000*, pages 343–350, 2000.
18. H. Löffelmann, H. Doleisch, and E. Gröller. Visualizing dynamical systems near critical points. In *Spring Conference on Computer Graphics and its Applications*, pages 175–184, Budmerice, Slovakia, 1998.
19. K. Mahrous, J. Bennett, B. Hamann, and K. Joy. Improving topological segmentation of three-dimensional vector fields. In *Data Visualization 2003. Proc. VisSym 03*, pages 203–212, 2003.

20. K. Mahrous, J. Bennett, G. Scheuermann, B. Hamann, and K. Joy. Topological segmentation in three-dimensional vector fields. *IEEE Transactions on Visualization and Computer Graphics*, 10(2):198–205, 2004.
21. P. A. Philippou and R. N. Strickland. Vector field analysis and synthesis using three dimensional phase portraits. *Graphical Models and Image Processing*, 59:446–462, November 1997.
22. G. Scheuermann, T. Bobach, H. Hagen K. Mahrous, B. Hamann, K. Joy, and W. Kollmann. A tetrahedra-based stream surface algorithm. In *Proc. Visualization 01*, pages 151 – 158, 2001.
23. G. Scheuermann, H. Krüger, M. Menzel, and A. Rockwood. Visualizing nonlinear vector field topology. *IEEE Transactions on Visualization and Computer Graphics*, 4(2):109–116, 1998.
24. H. Theisel. Designing 2D vector fields of arbitrary topology. *Computer Graphics Forum (Eurographics 2002)*, 21(3):595–604, 2002.
25. H. Theisel, Ch. Rössl, and H.-P. Seidel. Compression of 2D vector fields under guaranteed topology preservation. *Computer Graphics Forum (Eurographics 2003)*, 22(3):333–342, 2003.
26. H. Theisel and T. Weinkauf. Vector field metrics based on distance measures of first order critical points. In *Journal of WSCG*, volume 10:3, pages 121–128, 2002.
27. H. Theisel, T. Weinkauf, H.-C. Hege, and H.-P. Seidel. Saddle connectors - an approach to visualizing the topological skeleton of complex 3D vector fields. In *Proc. IEEE Visualization 2003*, pages 225–232, 2003.
28. X. Tricoche, G. Scheuermann, and H. Hagen. A topology simplification method for 2D vector fields. In *Proc. IEEE Visualization 2000*, pages 359–366, 2000.
29. X. Tricoche, G. Scheuermann, and H. Hagen. Continuous topology simplification of planar vector fields. In *Proc. Visualization 01*, pages 159 – 166, 2001.
30. J. van Wijk. Implicit stream surfaces. In *Proc. Visualization 93*, pages 245–252, 1993.
31. T. Weinkauf, H. Theisel, H.-C. Hege, and H.-P. Seidel. Boundary switch connectors for topological visualization of complex 3D vector fields. In *Data Visualization 2004. Proc. VisSym 04*, pages 183–192, 2004.
32. T. Weinkauf, H. Theisel, H.-C. Hege, and H.-P. Seidel. Topological construction and visualization of higher order 3D vector fields. *Computer Graphics Forum (Eurographics 2004)*, 23(3):469–478, 2004.
33. R. Westermann, C. Johnson, and T. Ertl. Topology-preserving smoothing of vector fields. *IEEE Transactions on Visualization and Computer Graphics*, 7(3):222–229, 2001.
34. T. Wischgoll and G. Scheuermann. Detection and visualization of closed streamlines in planar flows. *IEEE Transactions on Visualization and Computer Graphics*, 7(2):165–172, 2001.

(a) All 452 critical points (all of them are saddles) are located in a rather small area of the whole domain.

(b) 218 attracting and 234 repelling separations surfaces at a coarse resolution.

(c) 500 stream lines seeded homogeneous in the whole domain.

(d) 1023 saddle connectors have been extracted.

(e) 500 stream lines seeded near critical points.

Fig. 5. Flow around a backward-facing step.

Fig. 6. Simple topological skeleton consisting of 4 saddles; the 6 resulting sectors of different flow behavior can hardly be distinguished.
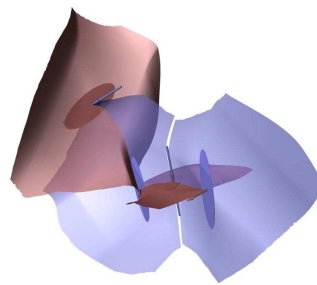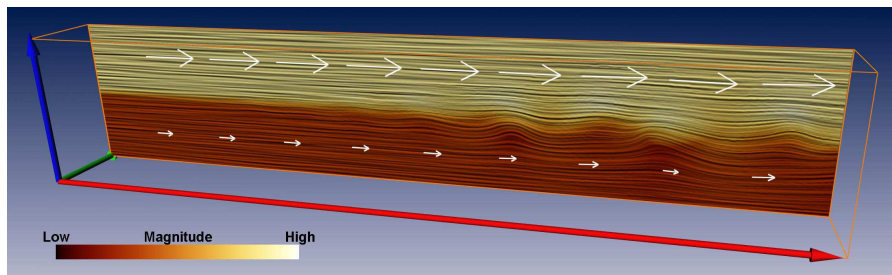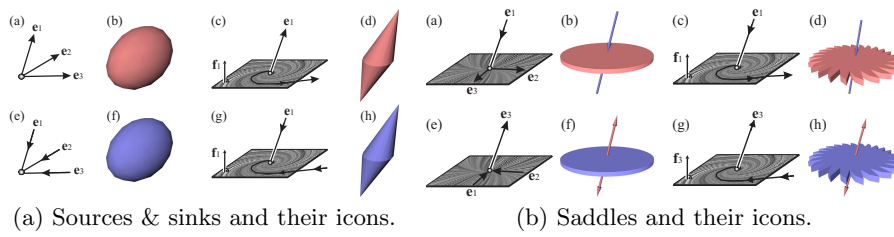
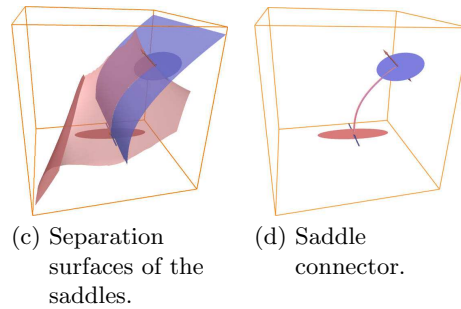(a) Original frame of reference. No critical points are present.
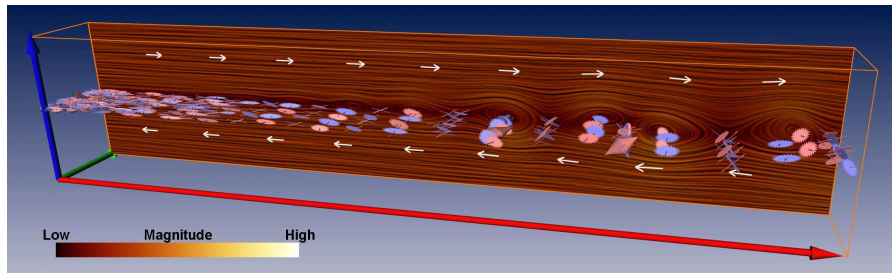
(b) Frame of reference chosen such that both layers have the same magnitude. 348 saddle points have been detected.

Fig. 7. Mixing layer.

(a) Sources & sinks and their icons.   (b) Saddles and their icons.

(c) Separation surfaces of the saddles.   (d) Saddle connector.

Fig. 8. Critical points and definition of saddle connectors.